Electronic topological transition in zinc metal at high external pressure

1996 J. Phys.: Condens. Matter 8 3581

(http://iopscience.iop.org/0953-8984/8/20/006)

J. Phys.: Condens. Matter **8** (1996) 3581–3599. Printed in the UK

Electronic topological transition in zinc metal at high external pressure

M Steiner†, W Potzel†, H Karzel†, W Schiessl†, M Köfferlein†, G M Kalvius† and P Blaha‡

† Physik-Department E15, Technische Universität München, D-85747 Garching bei München, Germany

‡ Institut für Technische Elektrochemie, Technische Universität Wien, A-1060 Wien, Austria

Received 26 January 1996

Abstract. We report investigations of Zn metal under quasi-hydrostatic pressures up to 16 GPa by ^{67}Zn Mössbauer spectroscopy and scalar–relativistic linearized augmented plane wave (LAPW) calculations. Our studies show that at 4.2 K an electronic topological transition (ETT) occurs at about 6.6 GPa, corresponding to a volume change of $(1-V/V_\circ) \approx 0.085$. At the ETT conduction electron states in the third Brillouin zone at the symmetry point L ('butterflies') move below the Fermi surface and start being occupied. At the ETT the electric field gradient tensor and the s electron density $\rho(0)$ at the ^{67}Zn nucleus remain virtually unchanged, but the lattice dynamics is drastically affected. The Lamb–Mössbauer factor (LMF) abruptly drops by a factor of two between 6.5 and 6.7 GPa and the curvature of the pressure dependence of the second-order Doppler shift (S_{SOD}) changes markedly. The results on LMF and S_{SOD} are described by a sudden destruction of a giant Kohn anomaly which accompanies the ETT.

1. Introduction

The behaviour of the electronic structure of hexagonal close-packed (hcp) metals has been of central interest in various experimental [1–3] and theoretical [4–7] investigations. Of particular importance are systems like Zn and Cd with unusually large c/a ratios which are far above the ideal value $c/a = (8/3)^{1/2} \approx 1.633$. As a consequence many solid-state properties are highly anisotropic [3, 5, 8, 9]. In addition, the non-spherical distribution of conduction electrons plays an important role. They are, for example, responsible for a pronounced electric field gradient (EFG) tensor at the nuclei of the lattice atoms. Most of these properties are well understood and can be calculated theoretically. Modern band-structure calculations are able to describe EFGs for all hcp elementary metals, including Zn, in good agreement with experiment [5].

However, the electronic subsystem does not only determine hyperfine interactions but also influences the lattice dynamics in an essential manner. A strong structural anisotropy in hexagonal metals is expected to lead to a close compensation of the two main contributions to the interionic interaction, the direct Coulomb ion–ion interaction and the indirect interionic interaction via conduction electrons [1, 10]. Clearly, if one of these contributions is changed, the total interionic interaction can be strongly affected. Such a change can drastically influence *low-frequency* phonons [10]. In a recent publication [11] we have demonstrated that these types of effects occur in Zn metal under external pressure, where at about 6.6 GPa the Lamb–Mössbauer factor abruptly drops by a factor of two. In addition, it was

0953-8984/96/203581+19$19.50

concluded in [12] that this drop is connected to a degeneracy of the magnitudes of several reciprocal lattice vectors at $c/a = \sqrt{3}$.

^{67}Zn Mössbauer spectroscopy is an excellent method to follow such changes of lattice dynamic behaviour. Due to the relatively low mass of ^{67}Zn and the rather high transition energy (93.31 keV) of the Mössbauer resonance the recoil-free fraction f (the Lamb–Mössbauer factor (LMF)) is small, only about 0.5% if an effective Debye temperature of $\theta_{eff} = 230$ K is assumed, which is typical for Zn metal [13]. This makes the observation of the resonance difficult and in general requires that the measurement be performed at liquid-helium temperatures. On the positive side, it is just the smallness of the LMF which makes it highly sensitive to lattice dynamic effects. In addition, in the low-temperature limit the LMF weights the phonon frequency distribution by ω^{-1} and thus provides increased sensitivity for changes of the phonon distribution at low frequencies. A further parameter which can give valuable information on lattice dynamics is the second-order Doppler shift S_{SOD}. In a Mössbauer experiment the experimentally determined centre shift S_C is the sum of the isomer shift S and S_{SOD}. Contrary to many other isotopes where $|S_{SOD}| \ll |S|$, for the 93.31 keV transition in ^{67}Zn both quantities can be comparable in size. Recently, a number of theoretical calculations for various zinc systems has been published to determine S [13–15]. This makes S_{SOD} available as an additional sensitive tool for lattice dynamics. In the low-temperature limit S_{SOD} weights the phonon spectrum by ω^{+1}. Thus S_{SOD} is more sensitive to changes of the phonon distribution at higher frequencies.

In the present paper we report for Zn metal the observation of an electronic topological transition (ETT) by which the polarization (screening of Zn ions) of conduction electrons is drastically changed. This in turn strongly affects the indirect interionic interaction and the low-frequency phonon distribution and leads to pronounced changes of the LMF and of S_{SOD} in ^{67}Zn Mössbauer high-pressure measurements. We have performed scalar–relativistic linearized augmented plane wave (LAPW) calculations which successfully describe the changes of the band structure at the ETT, of the electric field gradient tensor and of the s electron density $\rho(0)$ at the ^{67}Zn nucleus when high external pressure is applied.

2. Experimental details

2.1. A ^{67}Zn Doppler–velocity spectrometer for high pressures

For ^{67}Zn Mössbauer experiments at 4.2 K and pressures up to 8.5 GPa we used the spectrometer described in detail in [13, 16]. The pressure is applied to the ^{67}Zn metal absorber by two symmetrical B_4C anvils. The relatively large dimensions of the ^{67}Zn metal foil (enrichment about 91 at.% ^{67}Zn) of 4.0 mm diameter and 0.75 mm thickness required the application of a sandwich gasket [16]. It consisted of four pyrophyllite and three tantalum rings, each of 0.2 mm and 0.1 mm thickness, respectively. The gasket, which was centred by a Cu–Be extrusion ring, serves in addition as collimator for the 93.3 keV γ-radiation. As pressure transmitting medium we used Ag_2SO_4 which is characterized by a low shear modulus [17]. The pressure at the sample was determined *in situ* by a lead manometer [16, 18] which uses the known pressure dependence of the superconducting transition temperature of lead [19] as a gauge. From the exact shape of the resistance transition curve the pressure gradient over the absorber can be determined. We reached quasi-hydrostatic pressures up to 8.5 GPa with gradients smaller than 6%.

For the pressure range between 8.5 and 16 GPa we built a new type of high-pressure cell with sintered diamond anvils. This material can stand pressures up to 7000 N mm^{-2}, almost four times as much as B_4C. The dimensions of the ^{67}Zn metal absorber were reduced to

2 mm diameter and 0.5 mm thickness. The sandwich gasket consisted in this case of three pyrophyllite and two tantalum rings, each of 0.13 mm and 0.10 mm thickness, respectively. The pressure transmitting medium was again Ag_2SO_4. The pressure at 4.2 K was determined *in situ* by ^{197}Au-Mössbauer spectroscopy on a 10 μm thick Au foil which was situated close to the ^{67}Zn metal sample in the high-pressure cell. The pressure is derived from the known pressure dependence of the centre shift of metallic Au [20]. Further details of the sintered diamond anvil cell will be presented in a forthcoming publication [17]. The ^{197}Au measurements are not sensitive enough to derive information on the pressure gradient, for example from the linewidth of the absorption line of metallic gold. However, from the linewidth of the ^{67}Zn Mössbauer spectra we estimate a pressure gradient across the absorber of $\leqslant 10\%$ at 16 GPa. This again proves Ag_2SO_4 as a good pressure transmitting medium.

The B_4C or the sintered diamond anvil cells are mounted inside a Cu–Be clamp. The pressure generating force is applied to the sample at room temperature by means of a hydraulic press and then stored by heavy springs. The piezoelectric quartz drive producing Doppler velocities in the micrometre range is tightly fastened to the top of the pressure clamp. The Doppler drive acts on the source. In order to decouple the spectrometer from mechanical vibrations of the cryostat and of the boiling helium the whole system is suspended by springs inside a sealed stainless-steel dewar filled with He exchange gas [3, 16] and cooled to liquid-helium temperatures in a He-bath metal cryostat.

2.2. Source and absorber preparation

As the source we used ^{67}Ga in Cu, which shows a single emission line [21]. The ^{67}Ga ($T_{1/2} = 78$ h) activity was produced *in situ* by 46 MeV α bombardment of Cu discs with natural abundance of the Cu isotopes in the cyclotron KIZ of the Forschungszentrum Karlsruhe. The discs had 0.5 mm thickness and diameters of 8 mm and 5 mm for the B_4C anvil and sintered diamond anvil cells, respectively. The sources were used without annealing 48 h after irradiation to allow unwanted short-lived activities to decay.

For the ^{197}Au pressure calibration measurements we used the β^- decay of ^{197}Pt ($T_{1/2} = 18.3$ h). The ^{197}Pt activity was obtained by neutron activation of an enriched (90%) ^{196}Pt metal foil in the Forschungsreaktor München. The foils had a diameter of about 5 mm and a total weight of about 30 mg.

The ^{67}Zn metal absorber was produced by melting isotopically highly enriched Zn powder (about 91 at.% ^{67}Zn) at 870 K in a graphite crucible sealed within a quartz ampoule filled with argon gas. After melting the thin oxide layer was mechanically removed. The material was then rolled to prepare discs of 0.25 mm thickness and of 4 mm and 2 mm diameter for the B_4C anvil and sintered diamond anvil cells, respectively. The corresponding absorber thicknesses are 0.32 and 0.16 g cm^{-2} of ^{67}Zn metal. Before using the ^{67}Zn metal absorbers in the high-pressure experiments, they were characterized by ^{67}Zn Mössbauer measurements at ambient pressure.

2.3. Velocity calibration and nuclear pulse counting

The spectrometer was calibrated using the known quadrupole splittings in ^{67}Zn metal and in ^{67}ZnO at ambient pressure [22–24]. The γ-rays were detected by an intrinsic Ge diode of 10 mm thickness and 40 mm diameter coupled to a fast nuclear pulse counting chain [25]. Typical count rates in the 93.3 keV window were 72000 s^{-1} and 20000 s^{-1} for the B_4C and diamond anvil cells, respectively, at a signal-to-background ratio of $S/(S+B) \approx 74\%$. The data pulses were collected in time mode into a 512-channel analyser [26].

Although the tantalum discs of the sandwich gasket and the pressure transmitting medium (Ag_2SO_4) are very effective collimators, we found the gasket not to be thick enough to provide perfect collimation. However, since the geometrical arrangement of our experimental set-up is well characterized we were able to take this effect into account by numerical calculation [30]. In section 4.1 (table 1) we give the uncorrected as well as the corrected values for the $S/(S+B)$ ratios.

3. LAPW method

Our band structure calculations employ the full-potential linearized augmented plane wave (LAPW) method based on density functional theory [5, 27]. A fully relativistic description for the core states, but a scalar–relativistic description, neglecting spin–orbit coupling, for the valence states is used. Exchange and correlation are taken into account within the local density approximation, where the exchange potential is determined by the density of the electron gas in the crystal. This density is calculated self-consistently and allows one to derive the EFG tensor in an *ab initio* procedure. There is no need (and no possibility) to assume point charges or Sternheimer antishielding factors. We have used the computer code WIEN93 which comprises an improved and updated Unix version of the original copyrighted WIEN code [28]. We used the compressibility data for Zn metal of [29]. To obtain reliable results we applied a dense $\boldsymbol{k}$ mesh of 12000 points in the full Brillouin zone.

4. Results

4.1. Mössbauer measurements

Figure 1 shows Mössbauer absorption spectra recorded at 4.2 K and various pressures. Due to the quadrupole interaction, the spin-5/2 ground state of ^{67}Zn splits into three sublevels (the spin-1/2 excited state remains unchanged) which give rise to three absorption lines. The spectra were fitted by a superposition of three Lorentzians. The results are summarized in table 1. After finishing the high-pressure runs the cells were opened and the dimensions of the absorber remeasured. In all cases the area of the absorber foil has increased. The values n for the absorber thickness which are also given in table 1 were obtained by assuming that the area increases linearly with pressure.

The pressure dependences of the Lamb–Mössbauer factor (LMF), the centre shift (S_C) and of the quadrupole frequency ($\nu_Q = eQV_{zz}/h$) are given in table 2 and in figures 2–4.

The LMF f is derived form the total area under the three absorption lines after correction for background radiation. At first the LMF drastically increases from $f = 0.31(1)\%$ to $f = 1.41(15)\%$ at 6.5 GPa. Surprisingly, between 6.5 and 6.7 GPa f drops by a factor of two and increases again at higher pressures. This sudden reduction has been observed twice (see figure 2), with two set-ups of B_4C high-pressure cells of the same kind.

As shown in figure 3, the centre shift S_C decreases from 14.74(3) μm s^{-1} at ambient pressure to 0.79(28) μm s^{-1} at 16.0 GPa. There is, however, no abrupt change between 6.5 and 6.7 GPa.

Figure 4 demonstrates that also the quadrupole frequency $\nu_Q = eQV_{zz}/h$ strongly decreases from $\nu_Q = 12.45(2)$ MHz at ambient pressure to $\nu_Q = 5.07(20)$ MHz at 16.0 GPa. V_{zz} is the main component of the electric field gradient tensor. $Q = 0.150(15)$ b is the nuclear quadrupole moment [31]. The asymmetry parameter is $\eta = 0$ at all pressures. Also ν_Q does not show an abrupt change between 6.5 and 6.7 GPa.

Table 1. Summary of measured Mössbauer parameters for ^{67}Zn metal at 4.2 K and various pressures. Only statistical errors are quoted for position, width and area. The column for the absorber thickness n (in units of 10^{21} ^{67}Zn atoms/cm^2) also includes symbols for the two B_4C anvil cells (□, ○) and for the sintered diamond anvil cell (△) used in the high-pressure experiments. The signal-to-background ratio $(S/(S+B))_{corr}$ has been obtained from $(S/(S+B))_{meas}$ taking non-ideal collimation of the 93.3 keV γ-rays into account.

P (GPa)	Area (% μm s^{-1})	Width (μm s^{-1})	Position (μm s^{-1})	n (10^{21} ^{67}Zn cm^{-2})	$\left(\frac{S}{S+B}\right)_{meas}$ (%)	$\left(\frac{S}{S+B}\right)_{corr}$ (%)
0	0.068(7)	2.57(35)	−26.54(12)	5.859(43)	67.4	–
	0.060(5)	1.39(16)	+23.001(56)			
	0.044(5)	2.01(29)	+47.42(10)			
5.18(15)	0.097(21)	3.07(87)	−21.30(29)	3.14(19) (○)	76.3	60.0
	0.100(19)	2.59(67)	+13.49(23)			
	0.111(26)	4.9(1.5)	+29.75(49)			
5.93(23)	0.136(28)	5.0(1.3)	−20.49(39)	2.97(22) (○)	77.7	61.1
	0.101(17)	2.24(50)	+12.09(17)			
	0.130(33)	7.7(2.3)	+28.59(71)			
6.46(13)	0.149(19)	2.57(43)	−20.15(14)	3.22(18) (□)	72.4	57.0
	0.148(15)	1.74(25)	+12.433(84)			
	0.118(22)	4.08(99)	+28.97(33)			
6.68(35)	0.070(16)	2.14(66)	−20.60(22)	2.80(22) (○)	81.3	64.0
	0.104(17)	2.34(53)	+11.65(18)			
	0.042(20)	3.5(2.1)	+27.85(70)			
8.17(44)	0.089(25)	6.52(83)	−15.3(1.3)	2.87(24) (□)	79.5	62.6
	0.117(24)	6.52(83)	+10.2(1.0)			
	0.043(26)	6.52(83)	+24.2(2.5)			
8.34(43)	0.034(18)	1.7(1.2)	−15.93(50)	2.83(24) (□)	73.7	58.0
	0.065(14)	1.06(54)	+9.03(15)			
	0.042(14)	1.00(64)	+21.42(24)			
8.46(49)	0.065(27)	7.9(4.0)	−19.5(1.2)	2.81(20) (□)	71.0	55.9
	0.069(10)	1.47(28)	+8.704(99)			
	0.065(13)	2.70(72)	+21.92(24)			
13.1(1.2)	0.033(10)	1.066(82)	−15.00(17)	1.49(15) (△)	72.0	45.8
	0.023(11)	1.066(82)	+6.04(26)			
	0.033(11)	1.066(82)	+16.48(21)			
16.0(1.5)	0.022(15)	2.0(1.9)	−16.02(64)	1.49(15) (△)	69.4	44.1
	0.040(14)	1.6(1.0)	+4.31(26)			
	0.054(20)	3.1(1.5)	+14.09(51)			

4.2. LAPW calculations

Figure 5 shows the partial density of states (DOS) for 4s, 4p$_x$(p$_y$), 4p$_z$ and 3d electrons for two different values for the unit cell volume, $V = 201$ a.u.^{3}, $c/a = 1.86$ (ambient pressure) and $V = 161$ a.u.^{3}, $c/a \approx 1.65$ ($p \approx 24$ GPa). Several features are immediately apparent:

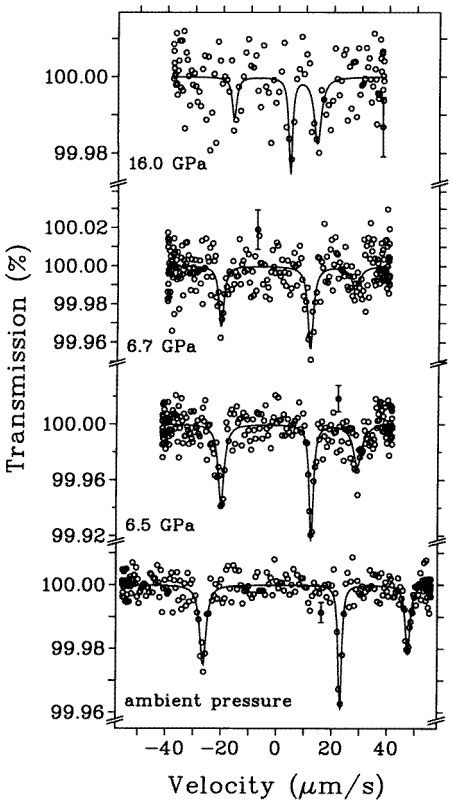

Figure 1. ^{67}Zn Mössbauer spectra of ^{67}Zn metal at 4.2 K and various pressures. The source is ^{67}Ga in Cu also at 4.2 K.

Table 2. Pressure dependence of the Lamb–Mössbauer factor f, the centre shift S_C and the quadrupole frequency $\nu_Q = eQV_{zz}/h$. At all pressures investigated we found the asymmetry parameter to be $\eta = 0$.

Pressure (GPa)	f (%)	S_C (μm s^{-1})	ν_Q (MHz)
0	0.312(12)	14.741(29)	12.447(20)
5.18(15)	1.02(16)	7.32(20)	8.64(13)
5.93(23)	1.26(22)	6.73(28)	8.19(16)
6.46(13)	1.41(15)	7.08(12)	8.194(73)
6.68(35)	0.75(14)	6.30(25)	8.10(13)
8.34(61)	0.687(78)	4.69(17)	6.38(13)
13.1(1.2)	0.81(19)	2.51(13)	5.27(10)
16.0(1.5)	1.10(30)	0.79(28)	5.07(20)

when the unit cell volume is reduced the width of the highest occupied band increases by 2 eV, the centre of the d band moves to lower energies, within an energy range of about 5 eV below the Fermi energy E_F the density of p states is increased at the expense of s electron states and the pronounced anisotropy of the p-states (p_x and p_y versus p_z) is

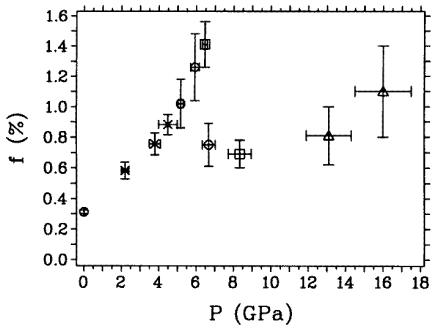

Figure 2. Pressure dependence of the Lamb–Mössbauer factor f. The drastic decrease between 6.5 and 6.7 GPa was reproduced with B_4C anvil cells in two set-ups of the same design (symbols □, ○). The results at the two highest pressures (△) were obtained in a sintered diamond anvil cell. Results of previous high-pressure ^{67}Zn Mössbauer measurements [3] (×) are also included.

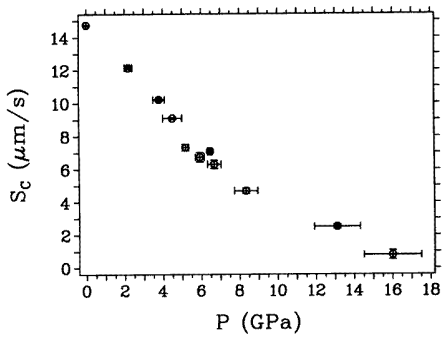

Figure 3. Pressure dependence of the centre shift S_C for ^{67}Zn metal at 4.2 K. The shift is given relative to a ^{67}Ga in Cu source also at 4.2 K.

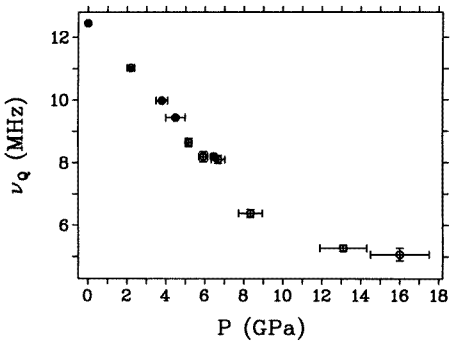

Figure 4. Pressure dependence of the quadrupole frequency $\nu_Q = eQV_{zz}/h$ of ^{67}Zn metal at 4.2 K. The asymmetry parameter η was found to be zero at all pressures investigated.

reduced.

Figure 6 depicts the energy bands for $V = 201$ a.u.^{3}, $c/a = 1.86$ and $V = 161$ a.u.^{3}, $c/a = 1.65$ and reveals a clear broadening with reduced volume. To mark the changes more clearly the region around E_F has been magnified in figure 7. To emphasize the character of the electronic wave functions circles with radii proportional to the respective partial charges are used in plotting the bands. The energy as well as the character change markedly between the symmetry points Γ and M, at Γ, at H, and between K and H. The 's band' originating at Γ rises in energy with pressure, while its p_z counterpart decreases. The $p_x(p_y)$ bands along K–H drop rapidly below E_F as does the s state at L at higher pressure. The situation at the symmetry point L is essential for the electronic topological transition. The energy change at the L point is given in table 3. Electron states at the L point cross E_F at a volume of $V \approx 178$ a.u.^{3}, where c/a is close to $\sqrt{3}$ as shown in recent x-ray diffraction experiments [12]. Table 3 also summarizes our theoretical results for the electric field gradient tensor

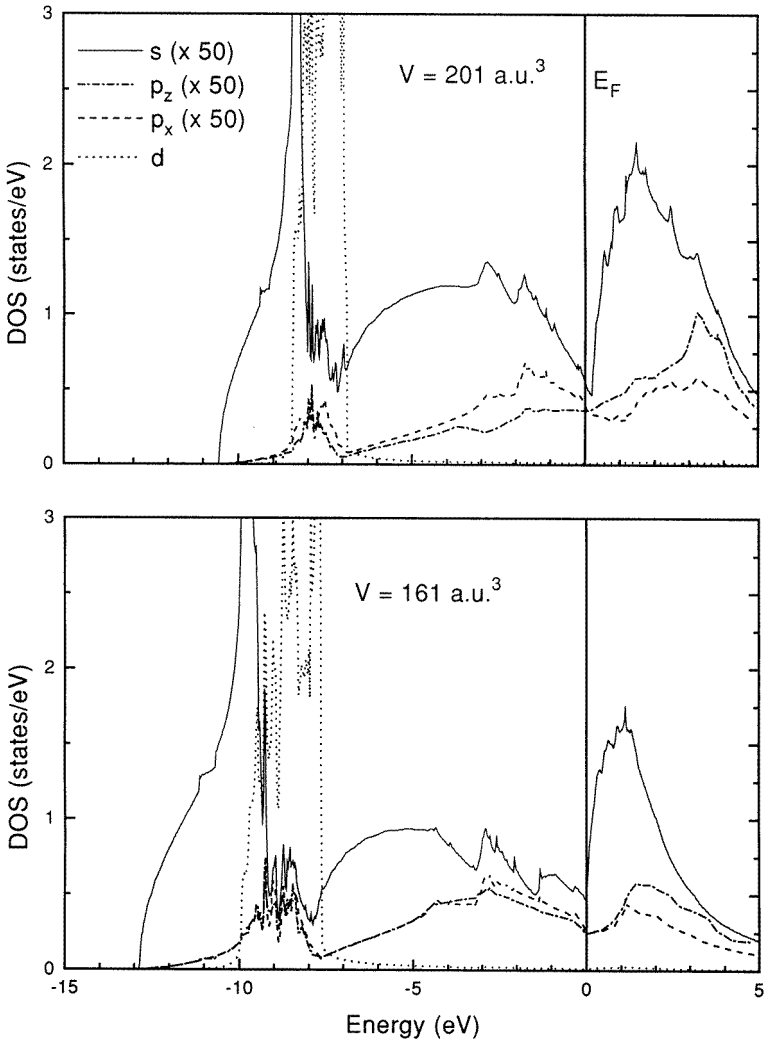

Figure 5. Partial density of states (DOS) for s, $p_x(p_y)$, p_z (multiplied by a factor of 50), and d electrons for two different values for the unit cell volume, $V = 201$ a.u.^{3}, $c/a = 1.86$ (ambient pressure) and $V = 161$ a.u.^{3}, $c/a \approx 1.65$ ($p \approx 24$ GPa).

and for the change of the s electron density $\rho(0)$ at the ^{67}Zn nucleus. Surprisingly $\rho(0)$ at first decreases when the unit cell volume is reduced and increases only when the volume is reduced below $V \approx 171$ a.u.^{3}. This decrease is mainly due to the valence (4s) electrons, the contribution originating from the core (1s, 2s, 3s) electrons decreases only slightly.

5. Discussion

5.1. The Lamb–Mössbauer factor

The volume dependence of the LMF is shown in figure 8. To convert pressure to volume changes we used the Murnaghan equation with a bulk modulus $B_\circ = 59$ GPa and its

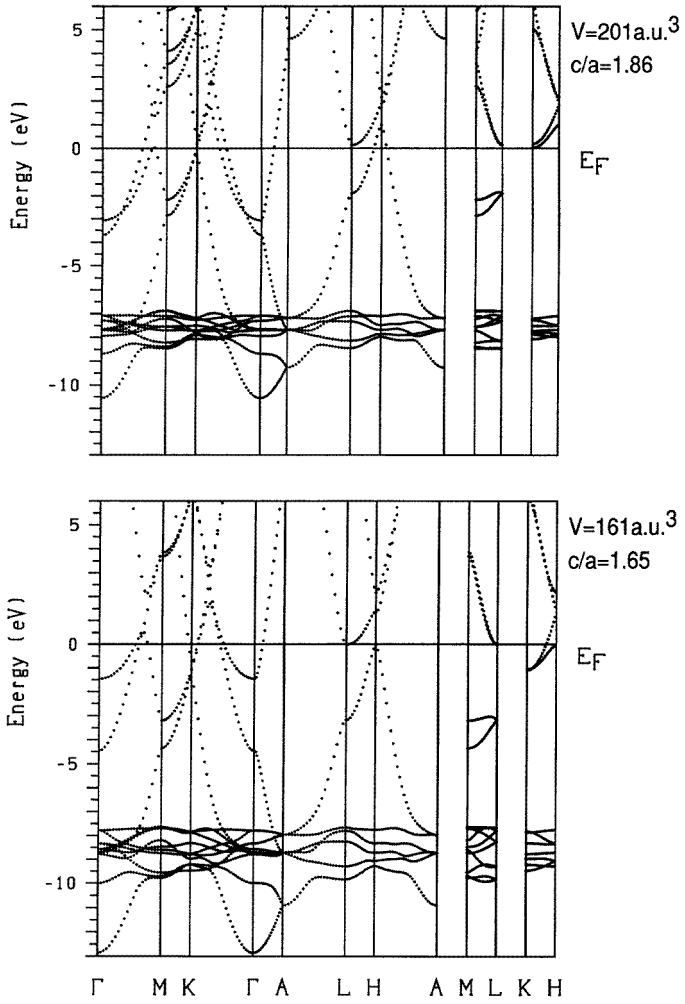

Figure 6. Energy bands for $V = 201$ a.u.^{3}, $c/a = 1.86$ and $V = 161$ a.u.^{3}, $c/a = 1.65$. The width of the bands broadens with reduced volume.

pressure derivative $B'_\circ = 5$ [29]. Some results of previous high-pressure ^{67}Zn Mössbauer measurements [3] are also included in figure 8. The main features are the drastic increase of the LMF by almost a factor of five and then the sudden drop at $(1 - V/V_\circ) = 0.085$. Let us first focus on the sharp drop. Compressibility data [12, 29] as well as the smooth variation of the centre shift S_C and of the quadrupole coupling frequency (see section 4.1) prove that there is no crystallographic phase transition in Zn metal at this volume reduction. Since the LMF is weighting the phonon frequency distribution by ω^{-1} in the low-temperature limit, the sharp drop indicates a drastic softening of low-frequency acoustic and optical phonons.

The highly anisotropic metals Zn and Cd have practically identical phonon dispersion relations if normalized with respect to the corresponding plasma frequencies. It turns out that the lattice dynamics is to a wide extent influenced by the interaction of phonons (wave vector $\boldsymbol{q}$) with conduction electrons (wave vector $\boldsymbol{k}_F$) at the Fermi surface. An essential feature of the band structure are the electronic states ('butterflies') in the third Brillouin

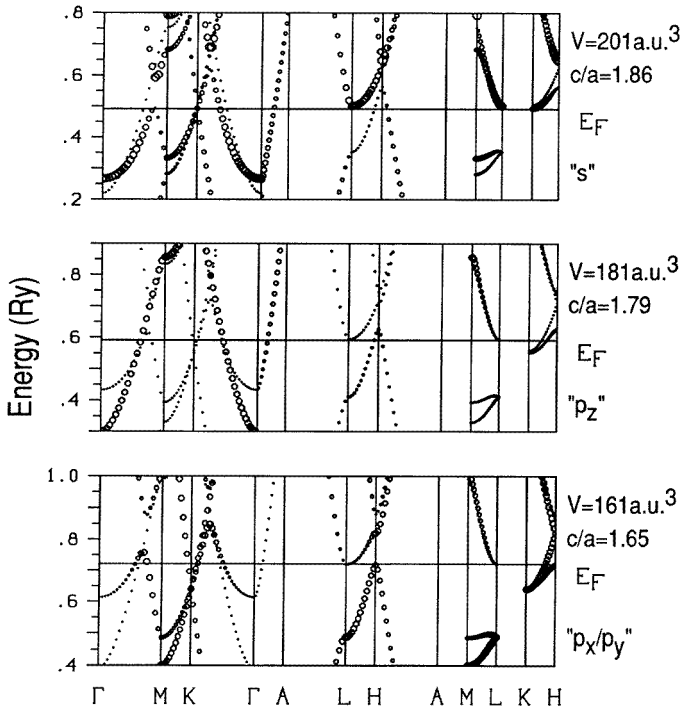

Figure 7. Energy bands around E_F for three volumes at experimental c/a values. The s, p_z and $p_x(p_y)$ character of the electronic wave function is proportional to the size of the circles used in plotting the bands for the three volumes. The energy as well as the character change markedly between the symmetry points Γ and M, at Γ, at H and between K and H. The situation at the symmetry point L is essential for the electronic topological transition: at a volume of $V \approx 178$ a.u.^{3} electron states at the symmetry point L cross E_F and an electronic topological transition occurs (see figure 9).

zone at the symmetry point L. Contrary to Mg metal with $c/a = 1.624$ [32] close to the ideal value, in Zn (and also Cd) metal these butterflies are not occupied [1, 10, 33]. The Fermi level E_F at the symmetry point L corresponding to the centre of the Brillouin zone boundary (101) lies in a local band gap close to its upper edge [1], namely there exists a locally empty and a locally fully occupied band above and below E_F, respectively. At the symmetry point L the Fermi surface and the Brillouin-zone boundary coincide. The maximal diameter of the Fermi surface in the direction of (101) is as large as the length of the reciprocal lattice vector $\boldsymbol{G}_L = (1, 0, 1)$. Such a situation leads to a giant Kohn anomaly in the long-wavelength regime [1, 10, 34].

5.1.1. The giant Kohn anomaly. Kohn anomalies reflect the interplay between phonons and conduction electrons at the Fermi surface [35]. For a nearly free electron gas, for example, they occur at $|\boldsymbol{q} + \boldsymbol{G}| = 2|\boldsymbol{k}_F|$, where $\boldsymbol{G}$ is a reciprocal lattice vector. If $|\mathbf{o}\boldsymbol{q}| \leqslant 2|\boldsymbol{k}_F|$, phonons $(\boldsymbol{q})$ connect electronic states $(\boldsymbol{k}_F)$ at the Fermi surface and cause electronic transitions with virtually no cost in energy. For $|\boldsymbol{q}| > 2|\boldsymbol{k}_F|$, however, electronic excitations are strongly impeded. This leads to a change of screening (polarization) of metal ions by conduction electrons which in turn abruptly changes the interaction between

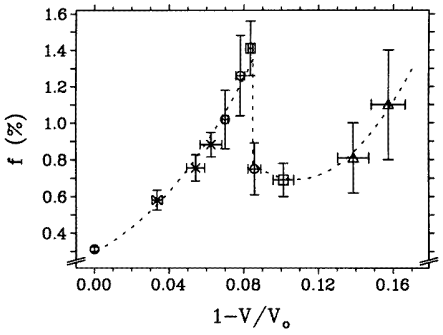

Figure 8. Volume dependence of the Lamb–Mössbauer factor f. Symbols as in figure 2. The dashed line through the data points is a guide to the eye only.

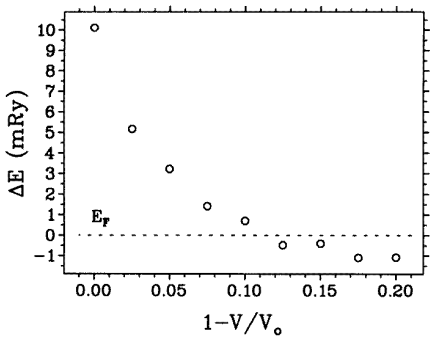

Figure 9. Results of scalar–relativistic LAPW calculations for the energy separation $\Delta E = E_L - E_F$ between the Fermi level E_F and the upper edge E_L of the local band gap at the symmetry point L. At $(1 - V/V_\circ) = 0.115$ E_L crosses E_F and an electronic topological transition occurs.

Table 3. Results of the LAPW calculations for Zn metal. Volume dependence of the c/a ratio (from [29]), of the Fermi energy E_F and the energy of the symmetry point L. $E_L - E_F \approx 0$ at a volume $V \approx 178$ a.u.^{3}. The changes of the electron densities at the ^{67}Zn nucleus are given with respect to their values at ambient pressure ($V = 201.093$ a.u.^{3}). The change of the total density at the nucleus $\Delta\rho(0)$ is the sum of the changes due to core electrons ($\Delta\rho^C(0)$) and valence electrons ($\Delta\rho^V(0)$). V_{zz} is the main component of the EFG tensor. In hcp symmetry the asymmetry parameter η is found to be $\eta = 0$ for all values of V.

V (a.u.^{3})	c/a	E_F (mRy)	E_L (mRy)	$E_L - E_F$ (mRy)	$\Delta\rho(0)$ (e/a.u.^{3})	$\Delta\rho^C(0)$ (e/a.u.^{3})	$\Delta\rho^V(0)$ (e/a.u.^{3})	V_{zz} (10^{17} V cm^{-2})
201.093	1.86	491.86	501.97	10.11	0	0	0	4.27
196.000	1.82	515.90	521.06	5.16	–0.049	–0.004	–0.045	3.63
191.040	1.79	540.45	543.67	3.22	–0.075	–0.010	–0.065	3.21
186.010	1.76	566.38	567.80	1.42	–0.095	–0.016	–0.079	2.77
180.980	1.73	593.28	593.98	0.70	–0.101	–0.025	–0.076	2.42
175.960	1.70	622.32	621.84	–0.48	–0.118	–0.035	–0.083	2.00
170.930	1.68	653.05	652.65	–0.40	–0.137	–0.048	–0.089	1.56
165.900	1.66	686.42	685.32	–1.10	–0.126	–0.064	–0.062	1.15
160.870	1.65	721.72	720.64	–1.08	–0.084	–0.083	–0.001	0.84

the partially shielded ions and thus influences the phonon spectrum. A giant Kohn anomaly can occur if—as in the example of Zn given above—for a certain $\boldsymbol{G}_\circ$ the Fermi surface lies in a local band gap with $2|\boldsymbol{k}_F| = |\boldsymbol{G}_\circ|$. As a consequence $|\boldsymbol{q}| \approx 0$, the anomaly then happens at long-wavelength acoustic and optical phonons and can be very pronounced. It has been called the 'giant Kohn anomaly' and is active within a small region of $\boldsymbol{q}$ vectors, $|\Delta\boldsymbol{q}| \propto 2V_{\boldsymbol{G}_\circ}/|\boldsymbol{G}_\circ|$, around $|\boldsymbol{q}| = 0$ [10]. $V_{\boldsymbol{G}_\circ}$ is the Fourier component of the effective electron–ion interaction corresponding to the reciprocal lattice vector $\boldsymbol{G}_\circ$. The position of E_F within the local band gap determines the influence of the giant Kohn anomaly on lattice dynamics. Theoretical calculations [10] predict that if E_F lies in the upper (lower) part of the gap the giant Kohn anomaly results in an extra hardening (softening) of low-frequency acoustic phonons. Such an effect has been estimated to be substantial, for example for the

elastic constant c_{44} in Cd [10].

5.1.2. Electronic topological transition. The extra hardening (softening) disappears abruptly when the giant Kohn anomaly is destroyed. In Zn metal this happens as a consequence of an electronic topological transition (ETT), when the topology of the Fermi surface is changed. Such an ETT has been observed for Cd metal under external pressure of 1.8 GPa via de Haas–van Alfvén measurements [36]. Our LAPW band-structure calculations show that an ETT also occurs in Zn metal under high external pressures.

Figure 9 depicts the results of our LAPW calculations. With decreasing unit cell volume, the separation ΔE between the upper edge of the local band gap and E_F is reduced. The upper edge reaches E_F at $(1 - V/V_\circ) \approx 0.115$. Here the topology of the Fermi surface abruptly changes. At the symmetry point L, states in the third Brillouin zone start being occupied. This ETT (Lifshitz transition) is accompanied by a destruction of the giant Kohn anomaly ('usual' Kohn anomalies, however, at $|\boldsymbol{q}| \neq 0$ are still present). The extra hardening is lost due to the change of indirect interaction between Zn ions via conduction electron screening. This strongly affects low-frequency phonons and in turn leads to a sudden drop of the LMF. The agreement between our theoretical (0.115) and experimental (0.085) values for $(1 - V/V_\circ)$ at which the ETT takes place is reasonable, considering that the calculations used c/a values obtained at room temperature [29]. A recent highly accurate x-ray diffraction experiment [12] at room temperature has shown that in the hcp structure a degeneracy of the magnitudes of several reciprocal lattice vectors occurs at $(1 - V/V_\circ) = 0.107$, where $c/a \approx \sqrt{3}$. Here the agreement with our LAPW calculations is even closer. Therefore, the observed singularity in the volume dependence of the c/a ratio is most probably connected to the ETT.

Let us now turn to the strong increase of the LMF which occurs before the ETT. Part of this increase originates from the extra hardening mentioned above which becomes more effective when the upper edge of the local band gap comes closer to E_F [10]. This, however, is probably not the only cause. In the low-temperature limit and for isotropic monatomic systems the volume dependence of the LMF is given by [30]:

$$\ln[f(V)] = \ln[f(V_\circ)]\left[1 + \gamma_{-1} \ln\left(\frac{V}{V_\circ}\right)\right] \tag{1}$$

where $V_\circ$ is the volume at ambient pressure and γ_{-1} is the (-1)th moment of the mode Grüneisen parameters $\gamma_j(\boldsymbol{q})$:

$$\gamma_{-1} = \frac{\sum_{\boldsymbol{q}j} \gamma_j(\boldsymbol{q})\omega_j^{-1}(\boldsymbol{q})}{\sum_{\boldsymbol{q}j} \omega_j^{-1}(\boldsymbol{q})} \tag{2}$$

with phonon frequency $\omega_j(\boldsymbol{q})$ characterized by wave vector $\boldsymbol{q}$ and branch j. The experimental results for $f(V)$ up to the ETT can very well be described by equation (1). A least-squares fit gives:

$$\gamma_{-1} = 3.42(18) \qquad f(V_\circ) = 0.293(18)\%. \tag{3}$$

The value for γ_{-1}, however, is rather large. It can be compared with results obtained from the effective Grüneisen parameter $\overline{\gamma}(T)$ in thermal expansion measurements:

$$\overline{\gamma}(T) = \frac{\int_0^{\omega_{max}} \mathrm{d}\omega\, \gamma(\omega) c_v(\omega/T) D(\omega)}{\int_0^{\omega_{max}} \mathrm{d}\omega\, c_v(\omega/T) D(\omega)} \tag{4}$$

where $\gamma(\omega)$ is a frequency dependent Grüneisen parameter. The specific heat is given by

$$c_v\left(\frac{\omega}{T}\right) = k_B \frac{(\hbar\omega/k_BT)^2 \exp(-\hbar\omega/k_BT)}{\left[1-\exp(-\hbar\omega/k_BT)\right]^2} \tag{5}$$

with $D(\omega)$ being the phonon frequency spectrum. Using data for $\overline{\gamma}(T)$ [39] and $D(\omega)$ [40, 41] it is possible to derive $\gamma(\omega)$ [30]. It turns out that $\gamma(\omega)$ is strongly frequency dependent.

We calculated the (-1)th moment according to

$$\gamma_{-1} = \frac{\int_0^{\omega_{max}} \mathrm{d}\omega\, \gamma(\omega)\omega^{-1}D(\omega)}{\int_0^{\omega_{max}} \mathrm{d}\omega\, \omega^{-1}D(\omega)} \tag{6}$$

where the integration extends over all phonon frequencies. We used $D(\omega)$ of [40], where $D(\omega)$ was experimentally derived from inelastic neutron scattering measurements. We obtain $\gamma_{-1} = 3.1(7)$ in close agreement with equation (3). Such high γ_{-1} values are not only found for Zn metal. In table 4 we summarize the corresponding parameters for all zinc containing materials on which high-pressure ^{67}Zn Mössbauer measurements have been performed. It appears that also α and β' brass exhibit large γ_{-1} values, whereas the semiconducting chalcogenides ZnO and ZnSe are characterized by considerably smaller numbers. It had already been shown in a previous publication [3] that the large γ_{-1} value for Zn metal cannot be explained by the large anisotropy. This is in accordance with the large γ_{-1} values found also for the cubic brass systems. Thus a large initial increase of the LMF with pressure might be a characteristic property of many metallic systems. Then conduction electrons are again the most likely cause. In this respect in Zn metal the K symmetry point is of particular interest. Electronic states ('needles') in this region of the Brillouin zone are increasingly populated when the c/a ratio is reduced under pressure. This can also lead to a pronounced hardening of the lattice [37]. It is not clear at present whether a corresponding electronic mechanism also prevails in the α and β' brass systems. However, ^{67}Zn Mössbauer experiments show that β' brass is unstable already at a very modest pressure of 1.1 GPa [38] and probably transforms into a crystallographic structure of lower symmetry. Then an increasing population of electronic states [37] analogous to the situation just described for Zn metal might be the origin of the rapid rise of the LMF with pressure.

Table 4. Results for γ_{-1} and $f(V_\circ)$ obtained from a least-squares fit of equation (1) to high-pressure ^{67}Zn Mössbauer data for various Zn containing systems.

	γ_{-1}	$f(V_\circ)$ (%)
Zinc metal	3.42(18)	0.293(18)
α-brass	3.51(90)	1.26(12)
β'-brass	3.53(36)	0.731(32)
ZnO	1.08(23)	2.0(2)
ZnSe	2.35(14)	0.49(2)

5.2. Centre shift

In a Mössbauer measurement the experimentally determined centre shift S_C is the sum of isomer shift S and second-order Doppler shift S_{SOD}. The latter is determined by lattice dynamics and can be expected to be influenced by the ETT. The main problem is the reliable

determination of S. The change ΔS with reduced volume is given by $\Delta S = \alpha \Delta\rho(0)$, where for ^{67}Zn the calibration constant $\alpha = (27.3 \pm 2.7)$ $a_\circ^3 \mu$m s^{-1} [14] and $\Delta\rho(0)$ is the change of the s electron density at the ^{67}Zn nucleus. We have determined $\Delta\rho(0)$ from our band structure calculations. Figure 10 shows our results for ΔS_C, ΔS and $\Delta S_{SOD} = \Delta S_C - \Delta S$. All shifts are plotted with respect to their values at ambient pressure. The change of isomer shift ΔS is discussed in section 5.3. With reduced volume the binding forces between Zn atoms are increased and ΔS_{SOD} becomes more negative. At $(1 - V/V_\circ) \approx 0.09$, the curvature of the ΔS_{SOD} curve changes sign, ΔS_{SOD} flattens and finally sharply decreases beyond $(1 - V/V_\circ) \approx 0.14$. The change in curvature of ΔS_{SOD} occurs at about the same volume reduction where the drop in the LMF (see figure 8) is observed and again reflects the softening of phonon modes at the ETT. The influence on ΔS_{SOD}, however, is much less pronounced than on LMF. This is expected, since in the low-temperature limit the LMF weights the phonon frequency distribution by ω^{-1} as compared to ω^{+1} in the case of S_{SOD} and is thus more sensitive to the low-frequency mode softening.

Due to the lack of experimental and theoretical data the change of S_{SOD} with pressure is sometimes estimated from the change of LMF by applying the Debye model [3, 13]. Such a procedure, however, may be too crude and lead to wrong results. In the case of Zn metal, for example, it predicts an increase of $\rho(0)$ with pressure. However, our LAPW calculations demonstrate that the opposite is true.

Similar to the case of the LMF (see equations (4)–(6)), S_{SOD} can be compared with results obtained from the effective Grüneisen parameter $\overline{\gamma}(T)$ in thermal expansion measurements.

In the limits of small volume compression and low temperature the volume dependence of S_{SOD} is given by [30]:

$$\Delta\tilde{S}_{SOD}(V) = -S_{SOD}(V_\circ)\gamma_{+1} \ln\left(\frac{V}{V_\circ}\right) \tag{7}$$

where

$$\gamma_{+1} = \frac{\int_0^{\omega_{max}} \mathrm{d}\omega\, \gamma(\omega)\omega^{+1} D(\omega)}{\int_0^{\omega_{max}} \mathrm{d}\omega\, \omega^{+1} D(\omega)}. \tag{8}$$

$\Delta\tilde{S}_{SOD}$ is determined by γ_{+1}, whereas the change in LMF (see equation (1)) is connected to γ_{-1}. For Zn metal, γ_{+1} and γ_{-1} differ by about a factor of two: $\gamma_{+1} = 1.2(4)$, $\gamma_{-1} = 3.1(7)$. Clearly, in such a situation of a large dispersion of the mode Grüneisen parameters the Debye model is bound to fail.

Using $D(\omega)$ of [40] we calculate $S_{SOD}(V_\circ) = -53.3 \mu$m s^{-1}. For small volume changes $[(1 - V/V_\circ) < 0.08]$ the agreement between $\Delta\tilde{S}_{SOD}$ obtained from equation (7) and ΔS_{SOD} (see figure 10) is close [30]. Thus the experimentally determined values for ΔS_C together with $\Delta\tilde{S}_{SOD}$ as derived via γ_{+1} from thermal expansion data are fully consistent with ΔS calculated theoretically with the LAPW procedure. In particular, they confirm the initial decrease of S.

5.3. Isomer shift

As demonstrated by figure 10 at first the isomer shift S (s electron density $\rho(0)$ at the ^{67}Zn nucleus) is reduced when the unit cell volume is compressed. Only above $(1 - V/V_\circ) \approx 0.15$ does S increase. A decrease of $\rho(0)$ with reduced volume is a rare case for pure elements. It has been observed for Sb [42] and β-Sn [43]. Usually in metallic systems $\rho(0)$ increases due to the compression of conduction electrons [44, 45]. Figure 11 exhibits the volume

dependence of the contact density of the core (1s, 2s and 3s electrons) and valence (4s) electrons. The decrease of $\rho(0)$ is primarily due to the valence electrons, the contribution of the core electrons decreases only slightly. From the DOS (figure 5) or bandstructure (figure 7) we can explain the unusual decrease of $\rho(0)$ by the s→p transfer of valence electrons. Especially between symmetry points Γ and M and between K and H bands with p character become occupied under pressure. The volume dependence of the valence electrons shows a small kink at $(1-V/V_\circ) \approx 0.10$, namely in the critical volume region where the ETT occurs. Thus the ETT is felt also by the isomer shift although the effect is not very pronounced. Above $(1 - V/V_\circ) \approx 0.15$, where the s→p transfer is nearly completed, the contribution of the valence electrons rapidly rises as usually expected.

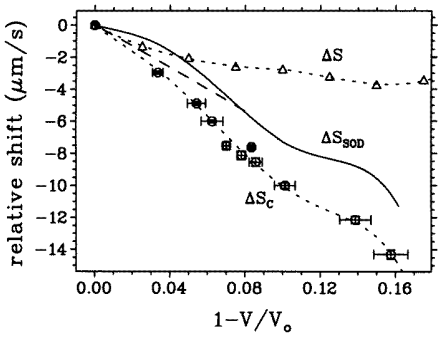

Figure 10. Volume dependence of the centre shift ΔS_C (○), the second-order Doppler shift ΔS_{SOD} (continuous line) and the isomer shift ΔS (△). All shifts are given with respect to their values at ambient pressure ($V = V_\circ$). ΔS_C is experimentally determined, ΔS is derived from our LAPW calculations, and $\Delta S_{SOD} = \Delta S_C - \Delta S$. The dotted lines are guides for the eye only. $\Delta \tilde{S}_{SOD}$ as derived from thermal expansion data via $\gamma_{+1} = 1.2(4)$ is indicated by the dashed line. $\Delta \tilde{S}_{SOD}$ and ΔS_C are consistent with the theoretically derived initial decrease of ΔS (see also figure 11).

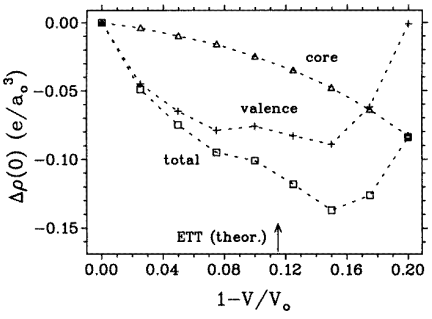

Figure 11. Results of our LAPW calculations for the volume dependence of the change of the s electron density $\rho(0)$ at the ^{67}Zn nucleus relative to $\rho(0)$ at ambient pressure. The contributions of the core electrons (△) and of the valence electrons (+) to the total (□) s electron density are indicated separately.

5.4. The electric field gradient tensor

Figure 12(a) shows our experimental and theoretical results for the main component V_{zz} of the EFG tensor. The relatively large experimental error bars are due to the uncertainty of the nuclear quadrupole moment [3]. The ETT which occurs at $(1 - V/V_\circ) \approx 0.085$ does not seem to have a strong influence on the EFG tensor (see below).

LAPW calculations [5] show that the main component V_{zz} of the EFG tensor at ambient pressure is mainly determined by local contributions, more distant contributions of the lattice give a correction of about 10% only. The main effect is caused by valence 4p electrons ($+53.1 \times 10^{16}$ V cm^{-2}) and valence 4d/3d electrons (-9.6×10^{16} V cm^{-2}), the semicore 3p (-0.3×10^{16} V cm^{-2}) and the lattice contributions (-5.7×10^{16} V cm^{-2}) being much smaller. At ambient pressure the population of $4p_x$ (and $4p_y$) electrons is larger by a factor of 1.47 than that of the $4p_z$ electrons. At a volume reduction of $(1 - V/V_\circ) \approx 0.080$ this factor is reduced to 1.05.

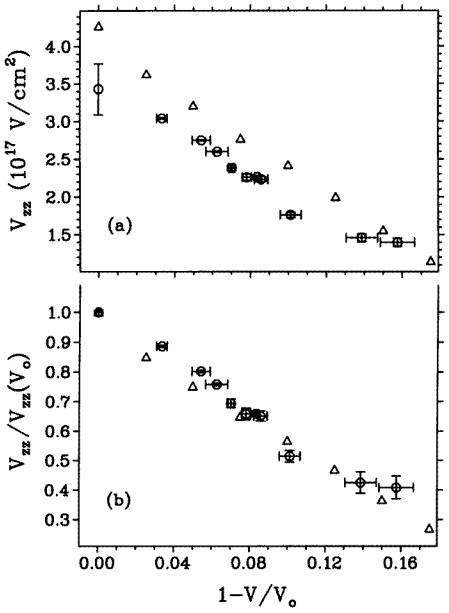

Figure 12. (a) Volume dependence of the main component V_{zz} of the electric field gradient tensor: experiment (○), LAPW calculation (△) using the room temperature structural parameters of [29]. The relatively large experimental error which is indicated only at ambient pressure is due to the uncertainty of the electric quadrupole moment Q of the ^{67}Zn nucleus. The differences between theory and experiment mainly originate from the fact that we had to use room temperature c/a values for our calculations. The uncertainty due to Q is eliminated in (b) where V_{zz} is normalized with respect to its value at ambient pressure.

The experimentally observed volume change of V_{zz} at constant temperature T is caused by two effects, the decrease of the c/a ratio and the reduction of the unit cell volume:

$$\left.\frac{\mathrm{d}\ln V_{zz}}{\mathrm{d}\ln V}\right|_T = \left.\frac{\partial \ln V_{zz}}{\partial \ln V}\right|_{T,c/a} + \left.\frac{\partial \ln V_{zz}}{\partial \ln[(c/a)-(c/a)_{ideal}]}\right|_{T,V} \left.\frac{\mathrm{d}\ln[(c/a)-(c/a)_{ideal}]}{\mathrm{d}\ln V}\right|_T . \tag{9}$$

Regarding the term $\left.\frac{\partial \ln V_{zz}}{\partial \ln V}\right|_{T,c/a}$ we have also calculated the volume dependence of V_{zz} keeping the c/a ratio constant at two different values:

$$\ln V_{zz} = 1.5111(7) - 1.550(8)\ln\left(\frac{V}{V_\circ}\right) \qquad \frac{c}{a} = 1.87 \tag{10}$$

$$\ln V_{zz} = 1.334(2) - 1.53(2)\ln\left(\frac{V}{V_\circ}\right) \qquad \frac{c}{a} = 1.828 \tag{11}$$

where V_{zz} is in 10^{17} V cm^{-2}. If hydrostatic pressure is applied such a decrease of the c/a ratio by about 0.04 would be accompanied by a volume change of $(1 - V/V_\circ) \approx 0.025$. Using experimental data for the volume dependence of the c/a ratio [29] we can solve for $\partial \ln V_{zz}/\partial \ln[(c/a) - (c/a)_{ideal}]$ in equation (9). For small volume changes we find that $\partial \ln V_{zz}/\partial \ln[(c/a) - (c/a)_{ideal}]$ decreases from 1.2 at ambient pressure to about 0.8 at $(1 - V/V_\circ) = 0.05$. Thus, the change of EFG with pressure is caused by two

counteracting effects: decreasing the volume increases the EFG with $\partial \ln V_{zz}/\partial \ln V \approx 1.5$ (see equations (10) and (11)), whereas decreasing the c/a ratio reduces the EFG with $\partial \ln V_{zz}/\partial \ln[(c/a)-(c/a)_{ideal}] \approx 1$. Considering, however, that for small volume reductions $\partial \ln[(c/a) - (c/a)_{ideal}]/\partial \ln V \approx 7$, the decrease of the EFG under external pressure is essentially determined by the decrease of the c/a ratio.

As figure 12(a) demonstrates the experimental values for V_{zz} are considerably lower than the results of the LAPW calculations. The main reason for this discrepancy is the fact that our calculations rely on room temperature structural data [29], whereas the ^{67}Zn Mössbauer experiments had to be performed at liquid-He temperatures where the lattice parameters are slightly different due to the (anisotropic) thermal expansion. The c/a ratio, for example, at 4.2 K and ambient pressure is $c/a = 1.828$ [46] versus 1.86 at room temperature [29]. If this is taken into account the agreement for the EFG value at ambient pressure is within about 10%, which is the accuracy of the quadrupole moment Q. To eliminate the uncertainty of Q, in figure 12(b) we have plotted the volume dependence of V_{zz} as obtained from experiment and LAPW theory, in each case normalized to the value of V_{zz} at ambient pressure.

In the experimental data, there appears to be a change in curvature at $(1-V/V_\circ) \approx 0.10$. Although the overall agreement between theory and experiment is satisfactory, this change in curvature is not present in our theoretical results. Again we surmise that this discrepancy originates from the use of room temperature structural data [29].

As already mentioned above, our experimental and theoretical data show that the ETT does not influence the EFG tensor in a profound manner. The reason is that the ETT abruptly changes the dynamic screening of the conduction electrons, whereas the band structure and thus the static electronic structure is altered only marginally. However, since the EFG is decisively determined by the c/a ratio the change in curvature close to the ETT in our experimental results does reflect a small, but anomalous change in the c/a ratio at 4.2 K. This raises the question of whether the ETT in Zn metal is connected to a structural phase transition.

5.5. The ETT and structural phase transition

A connection between an ETT and a structural phase transition has been observed in Cs metal which exhibits an isostructural (fcc–fcc) phase transition at room temperature between the two high-pressure modifications Cs(II) and Cs(III). Relativistic band structure calculations using the linear muffin tin orbital (LMTO) method in atomic sphere approximation [47] show that at a volume reduction of $(1 - V/V_\circ) \approx 0.52$ an ETT occurs which involves the X symmetry point. The isostructural phase transition is observed at somewhat larger volume reduction of $(1 - V/V_\circ) \approx 0.57$ [48–50]. In Cs metal, the ETT is the precursor of the isostructural phase transition. At the ETT the electronic contribution to the internal pressure markedly changes and causes a softening of phonon modes which finally leads to the isostructural phase transition.

Recent high-pressure x-ray diffraction experiments carried out with high precision at room temperature [12] give strong indications that for Zn metal the c/a ratio shows an anomaly at the ETT. Earlier x-ray experiments [29, 51] were not accurate enough to show this anomaly. The *high-precision* x-ray experiments [12] reveal that the volume dependence of the c/a ratio changes its slope at $(1 - V/V_\circ) = 0.107$, where $c/a = \sqrt{3}$. This volume change is slightly larger than the value $(1 - V/V_\circ) = 0.085$ where we find the ETT. The x-ray experiments, however, were performed at room temperature. As mentioned above (see section 5.4) the c/a ratio decreases to 1.828 at 4.2 K and ambient pressure [46] versus

1.86 at room temperature [29]. If we assume a similar volume dependence as in [12] at low temperature, the ETT observed in our Mössbauer experiments occurs very close to $c/a = \sqrt{3}$. Therefore, the anomaly in the c/a ratio at room temperature and the ETT observed at 4.2 K most probably have the same physical origin. Also the volume dependence of the EFG tensor (see section 5.4) is a hint that the ETT in Zn metal is connected to a change of the c/a ratio. From theoretical point of view, total energy calculations [7] using the LMTO method predict an anomalous behaviour in the c/a ratio in the volume range $[0.08 < (1 - V/V_\circ) < 0.10]$ where we observe the ETT. Our own total energy calculations do not show a significant c/a anomaly, but it should be mentioned that the theoretical c/a ratio is largely overestimated when using the standard local density approximation. Still, high-pressure x-ray or neutron diffraction measurements at low temperatures (4.2 K) are highly desirable to settle the question of whether the ETT and the anomaly of the c/a ratio occur exactly at the same volume reduction or whether the ETT might be the precursor of the structural changes as in Cs metal.

6. Conclusions

Our high-pressure Mössbauer data and scalar-relativistic LAPW calculations show that the conduction electrons decisively determine the lattice dynamics of Zn metal. An electronic topological transition which involves the L symmetry point causes the destruction of a giant Kohn anomaly and as a consequence drastically changes the lattice dynamics. It is demonstrated that ^{67}Zn Mössbauer spectroscopy is a powerful tool to follow such effects because of its high sensitivity with respect to the Lamb–Mössbauer factor. Since the same resonance due to its high relative energy resolution is also well suited for determining small energy changes of the 93.3 keV γ-rays, our experiments prove that the ETT hardly affects hyperfine interactions (isomer shift and EFG tensor) which are determined by static properties of the band structure. Our LAPW calculations do describe the electronic energy changes as well as isomer shifts and electric field gradients. However, first principles lattice-dynamic models are highly desirable to reproduce quantitatively the sudden changes observed for the LMF at the ETT.

Acknowledgments

We gratefully acknowledge most valuable discussions with Professor Yu Kagan, Kurchatov Institute Moscow. We would like to thank the Forschungszentrum Karlsruhe, especially Dr H Schweickert, K Assmus, and W Maier for the numerous and careful source irradiations at the cyclotron (KIZ). This work has been funded by the German Federal Minister for Research and Technology (Bundesminister für Forschung und Technologie (BMFT)) under Contract 03-KA3TUM-4 and the Forschungszentrum Karlsruhe.

References

[1] Ivanov A S, Mitrofanov N L, Pushkarev V V, Rumyantsev A Yu and Chernoplekov N A 1986 *Fiz. Tverd. Tela* **28** 767 (Engl. transl. 1986 *Sov. Phys.– Solid State* **28** 427)
[2] Potzel W, Adlassnig W, Närger U, Obenhuber Th, Riski K and Kalvius G M 1984 *Phys. Rev.* B **30** 4980
[3] Potzel W, Adlassnig W, Moser J, Schäfer C, Steiner M and Kalvius G M 1989 *Phys. Rev.* B **39** 8236
[4] Das T P and Schmidt P C 1986 *Z. Naturf.* a **41** 47
[5] Blaha P, Schwarz K and Dederichs P H 1988 *Phys. Rev.* B **37** 2792
[6] Blaha P 1990 *Hyperfine Interact.* **60** 773

[7] Meenakshi S, Vijayakumar V, Godwal B K and Sikka S K 1992 *Phys. Rev.* B **46** 14359
[8] Daniuk S, Jarlborg T, Kontrym-Sznajd G, Majsnerowski J and Stachowiak H 1989 *J. Phys.: Condens. Matter* **1** 8397
[9] Singh D and Papaconstantopoulos D A 1990 *Phys. Rev.* B **42** 8885
[10] Kagan Yu, Pushkarev V V and Holas A 1983 *Zh. Eksp. Teor. Fiz.* **84** 1494 (Engl. transl. 1983 *Sov. Phys.–JETP* **57** 870)
[11] Potzel W, Steiner M, Karzel H, Schiessl W, Köfferlein M, Kalvius G M and Blaha P 1995 *Phys. Rev. Lett.* **74** 1139
[12] Kenichi T 1995 *Phys. Rev. Lett.* **75** 1807 and private communication
[13] Potzel W 1993 *Mössbauer Spectroscopy Applied to Magnetism and Materials Science* vol 1, ed G J Long and F Grandjean (New York: Plenum) p 305
[14] Mitchell D W, Das T P, Potzel W, Kalvius G M, Karzel H, Schiessl W, Steiner M and Köfferlein M 1993 *Phys. Rev.* B **48** 16449
[15] Svane A and Antoncik E 1986 *Phys. Rev.* B **33** 7462
[16] Adlassnig W, Potzel W, Moser J, Schäfer C, Steiner M and Kalvius G M 1989 *Nucl. Instrum. Methods* A **277** 485
[17] Steiner M, Potzel W, Karzel H, Schiessl W, Köfferlein M, Kalvius G M and Blaha P 1996 to be published
[18] Willer J and Moser J 1970 *J. Phys. E: Sci. Instrum.* **12** 886
[19] Buchmann U 1985 *Diploma Thesis* Technische Universität Braunschweig
[20] Roberts L D, Patterson D O, Thomson J O and Levey R P 1969 *Phys. Rev.* **179** 656
[21] Potzel W, Forster A and Kalvius G M 1978 *Phys. Lett.* A **67** 421; 1979 *J. Physique. Coll.* **40** C2-29
[22] Potzel W, Obenhuber Th, Forster A and Kalvius G M 1982 *Hyperfine Interact.* **12** 135
[23] Obenhuber Th, Forster A, Potzel W and Kalvius G M 1983 *Nucl. Instrum. Methods* **214** 361
[24] Perlow G J, Potzel W, Kash R M and de Waard H 1974 *J. Physique Coll.* **35** C6-197
[25] Potzel W and Halder N 1984 *Nucl. Instrum. Methods* **226** 418
[26] Forster A, Potzel W and Kalvius G M 1980 *Z. Phys.* **B37** 209
[27] Blaha P, Schwarz K and Herzig P 1985 *Phys. Rev. Lett.* **54** 1192
[28] Blaha P, Schwarz K and Augustyn R 1993 Computer Code WIEN93, Technical University Vienna (an improved and updated Unix version of the original copyrighted WIEN code, which was published by Blaha P, Schwarz K, Sorantin P and Trickey S B 1990 *Comput. Phys. Commun.* **59** 399)
[29] Schulte O, Nikolaenko A and Holzapfel W B 1991 *High Pressure Res.* **6** 169
[30] Steiner M 1994 *PhD Thesis* Technische Universität München
[31] Laulainen N S and McDermott M N 1969 *Phys. Rev.* **177** 1606
[32] Wyckoff R W G 1965 *Crystal structures* vol 1, 2nd edn (New York: Wiley) p 11
[33] Watts B R and Mayers J 1979 *J. Phys. F: Met. Phys.* **9** 1565 and references therein
[34] Chernyshov A A, Pushkarev V V, Rumyantsev A Yu, Dorner B and Pynn R 1979 *J. Phys. F: Met. Phys* **9** 1983
[35] Kohn W 1959 *Phys. Rev. Lett.* **2** 393
[36] Bud'ko S L, Voronovskii A N, Gapotchenko A G and Itskevich E S 1984 *Zh. Eksp. Teor. Fiz.* **86** 778 (Engl. transl. 1984 *Sov. Phys.– JETP* **59** 454)
[37] Lifshitz I M, Rzhevskii V V and Tribel'skii M I 1981 *Zh. Eksp. Teor. Fiz.* **81** 1528 (Engl. transl. 1981 *Sov. Phys.– JETP* **54** 810)
[38] Adlassnig W, Potzel W, Moser J, Schiessl W, Potzel U, Schäfer C, Steiner M, Karzel H, Peter M and Kalvius G M 1989 *Phys. Rev.* B **40** 7469
[39] McCammon R D and White G K 1965 *Phil. Mag.* **11** 1125
[40] Eremeev I P, Sadikov I P and Chernyshov A A 1976 *Sov. Phys.– Solid State* **18** 960
[41] Raubenheimer L J and Gilat G 1967 *Phys. Rev.* **157** 586
[42] Krakow W T, Josephson W D, Deane P A, Williamson D L and Roberts L D 1981 *Phys. Rev.* B **23** 499
[43] Chow L, Deane P A, Farrell J N, Magill P A and Roberts L D 1986 *Phys. Rev.* B **33** 3039
[44] Kalvius G M, Klein U F and Wortmann G 1974 *J. Physique Coll.* **35** C6-139
[45] Gleissner A, Potzel W, Moser J and Kalvius G M 1993 *Phys. Rev. Lett.* **70** 2032
[46] Touloukian Y S, Kirby R K, Taylor R E and Desai P D (eds) 1975 *Thermophysical Properties of Matter* vol 12 (New York, Washington: IFI/Plenum)
[47] Glötzel D and McMahan A K 1979 *Phys. Rev.* B **20** 3210
[48] Kennedy G C, Jayaraman A and Newton R C 1962 *Phys. Rev.* **126** 1363
[49] McMahan A K 1978 *Phys. Rev.* B **17** 1521
[50] Boehler R and Ross M 1984 *Phys. Rev.* B **29** 3673
[51] Lynch R W and Drickamer H G 1965 *J. Phys. Chem. Solids* **26** 63